Journal of Colloid and Interface Science **236,** 141–154 (2001)
doi:10.1006/jcis.2000.7400, available online at http://www.idealibrary.com on IDEAL®

Forces between a Rigid Probe Particle and a Liquid Interface

I. The Repulsive Case

D. Y. C. Chan,[1] R. R. Dagastine, and L. R. White[2]

Center for Complex Fluids Engineering, Department of Chemical Engineering, Carnegie Mellon University, Pittsburgh, Pennsylvania 15213-3890

Received August 1, 2000; accepted December 18, 2000

The effect of disjoining pressure between a rigid spherical probe particle (attached to an AFM cantilever) and a liquid interface (e.g., oil/water or air/water) is treated in an analytic manner to describe the total force F exerted on the probe as a function of the distance X of the probe from the rigid substrate (AFM stage) on which the liquid interface resides. Two cases (i) a flat interface under gravity and (ii) a drop whose size is sufficiently small that gravity can be neglected have been examined. A simple numerical algorithm is given for computing $F(X)$ (the AFM observable) from a given form for the disjoining pressure. Numerical results are displayed for electrostatic probe/interface interactions which reveal the linear compliance regime experimentally observed in AFM experiments on these systems. The slope of the linear compliance regime is shown to be a function of the properties of the interface (capillary length, particle radius, drop size, contact angle of drop on rigid substrate etc.). © 2001 Academic Press

Key Words: **liquid interface; deformable interface; AFM; colloidal probe; constant compliance; oil drop; flat interface.**

1. INTRODUCTION

The interaction of solid colloidal particles with deformable liquid interfaces is of fundamental interest in technologically important areas such as flotation, deinking of paper, and water purification. The measurement of these forces by atomic force microscope (AFM) is becoming commonplace. Ducker *et al.* (1) measured forces across water between a silica particle attached to the AFM cantilever and an air bubble anchored to the piezo-driven stage. A similar experiment was reported by Fielden *et al.* (2), Butt (3), and Preuss and Butt (4). Measurements of forces between probe particle and sessile oil drops in water have recently been reported by Mulvaney *et al.* (5), Snyder *et al.* (6), and Hartley *et al.* (7). The interpretation of these measurements has been via a procedure introduced by Ducker *et al.* (1) which we describe below.

It should be appreciated that the display of force versus central separation distance, D_o, between probe particle surface and the surface of the liquid fixed to the movable stage can be achieved only by observing a "linear compliance" regime in the measurement. By this we mean that cantilever deflection d (as measured by a light reflection technique) is observed to asymptote to a linear behavior when plotted against stage displacement l (determined by piezo voltage). For a rigid substrate and probe, this linear regime is interpreted as the stage (i.e., substrate) and cantilever tip (i.e., probe particle) moving together. From Fig. 1 we observe that the separation distance between rigid particles and substrate is given by

$$D_o = d + l_o - l \qquad [1.1]$$

where

$$l_o = L - 2a - z_o. \qquad [1.2]$$

In general l_o is not a constant since the substrate is deformed by the force, F, exerted by the probe on the substrate. If the substrate is a linearly elastic body then we may write

$$F = -K_d\left(z_o - z_o^\infty\right), \qquad [1.3]$$

where z_o^∞ is the height of the undistorted substrate from the rigid stage so that $z_o - z_o^\infty$ is the central deformation of the substrate. The elastic properties of the substrate are contained in the effective "spring constant" K_d for the substrate. We also have that

$$F = K_c d, \qquad [1.4]$$

where K_c is the spring constant of the AFM cantilever. Substituting [1.4], [1.3], into [1.2] we have

$$l_o = l_o^\infty + \frac{K_c}{K_d} d, \qquad [1.5]$$

[1] Current address: Centre for Particulate Fluid Processing, Department of Mathematics and Statistics, University of Melbourne, Parkville 3052, Melbourne, Australia.

[2] To whom all correspondence should be addressed at Department of Chemical Engineering, Carnegie Mellon University, Doherty Hall, 5000 Forbes Avenue, Pittsburgh, PA 15213-3890.

0021-9797/01 $35.00

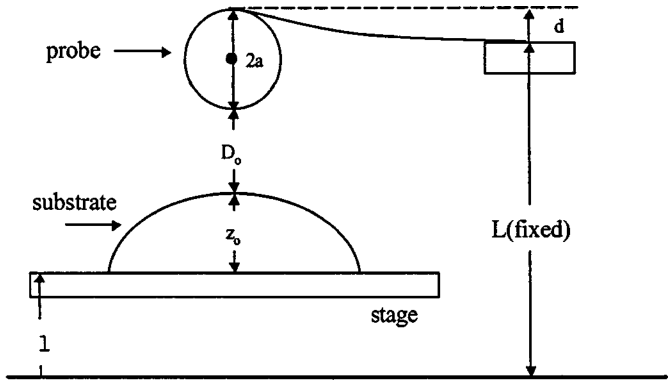

FIG. 1. Geometry of the AFM measurement.

where

$$l_o^\infty = L - 2a - z_o^\infty, \quad [1.6]$$

and [1.1] may be written as

$$D_o = \left(1 + \frac{K_c}{K_d}\right)d - l + l_o^\infty. \quad [1.7]$$

Experimentally, we observe at close separation of the surfaces an apparent "linear compliance" region where d is observed to vary linearly with l. Conventionally, this region is explained by invoking the onset of a short-range repulsive force (hard sphere overlap) with a very small decay length. At these separations, small separation decrease results in a large increase in the force F. Thus in this region, while the force F is accommodated by the substrate, D_o is effectively constant ($D_o = D_w$) and we see from [1.7], that

$$d = \frac{1}{\left(1 + \frac{K_c}{K_d}\right)}\left(l - \left(l_o^\infty - D_w\right)\right). \quad [1.8]$$

The slope of the linear compliance region is thus $(1 + K_c/K_d)^{-1}$ and the intercept on the l axis is $l_o^\infty - D_w$. Having determined these quantities from the linear compliance region, we may calculate D_o outside this region using [1.7] in the form

$$D_o = D_w + d\left(\frac{1}{\text{slope}}\right) - l + \text{intercept}. \quad [1.9]$$

For rigid interfaces, $K_d \gg K_c$, and hence the linear compliance region of a d vs l plot will have slope 1. Indeed the calibration factor for the conversion of split diode voltage to cantilever deflection may be calculated by requiring the slope to be unity in the linear compliance regime.

Since $D_w \sim 0.2$ nm for the onset of "hard sphere" overlap forces, D_w is usually neglected with respect to the typical D_o values corresponding to colloidal forces. Graphically, for a given deflection, d, the separation distance D_o is shown in Fig. 2 is the horizontal distance between the experimental d vs l curve and the extrapolated linear compliance line.

When AFM is employed to measure the surface forces at bubble/drop substrates with a rigid probe particle in situations where the colloidal forces are predominately repulsive, an apparent linear region (with a slope significantly less than one) in the d vs l curve is observed and the use of the above analysis to extract D_o values is immediately suggested. This is, in essence, the Ducker analysis (1) of bubble/drop systems. By assuming (i) that the drop behaves like a Hookean spring with an effective spring constant $K_d < K_c$ and (ii) that linearity is due to $D_o \approx D_w$ (constant), Ducker and later researchers were able to back out $F(D_o)$ curves (assuming $D_w \ll$ colloidal force range and could therefore be neglected).

The aim of the present paper is to elucidate the validity or otherwise of these assumptions. We analyze the action of inter-surface disjoining pressure on a deformable liquid interface and the consequences for AFM measurement of such forces. We will examine two limiting cases where the problem can be treated analytically in the most part. We consider a rigid spherical probe particle (radius a) interacting with

(a) a flat liquid interface where $D_o \ll a, \lambda$
(b) a drop (bubble) interface (radius R_o) such that $D_o \ll a < R_o \ll \lambda$.

Here D_o is a separation distance at which disjoining pressures manifest themselves and λ is the capillary length under gravity (g) of the interface, viz.

$$\lambda = \left(\frac{\gamma}{\Delta\rho g}\right)^{1/2}, \quad [1.10]$$

where γ is the interfacial tension and $\Delta\rho$ is the density difference between substrate and bathing medium. Since D_o is typically 10^{-9}_{m}, $a \sim 10^{-6}_{\mathrm{m}}$, and $\lambda \sim 10^{-3}_{\mathrm{m}}$ the above cases are

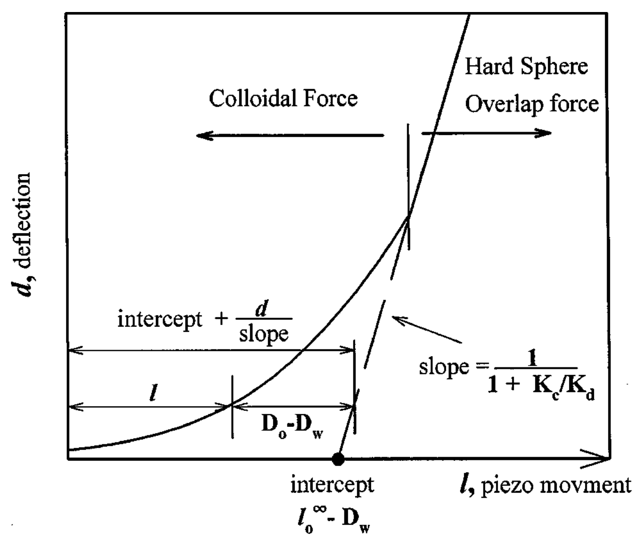

FIG. 2. The extraction of separation distance D_o from the linear compliance region.

not unnecessarily restrictive. Clearly for case (b) we should use drops (bubbles) with $R < 10^{-4}_{\mathrm{m}}$ (i.e., a tenth of a millimeter). We note that a similar treatment has been given earlier by Miklavcic and co-workers (8, 9) using a perturbation theory approach.

2. DEFORMATION OF THE LIQUID INTERFACE

We consider first the case of the infinite flat liquid surface. The interface here is flat due to the large volume of the substrate drop (or bubble) and the action of gravity. The geometry is shown in Fig. 3. We choose as a fundamental variable the vertical distance X between the origin fixed to the stage and the lowest point on the probe sphere as shown in Fig. 3. This quantity (or at least the change in ΔX from some reference point) is obtainable directly from AFM d versus l measurements since from Eq. [1.1],

$$X = z_o + D_o \qquad [2.1]$$

$$= X_o + d - l, \qquad [2.2]$$

where

$$X_o = L - 2a. \qquad [2.3]$$

Our aim is to calculate the force F exerted on the probe by the disjoining pressure from the liquid interface as a function of X. At radial distance r from the axis (see Fig. 3) the surface separation is $D(r)$ given by

$$D(r) = [r^2 + (X+a)^2 - 2(X+a)z(r) + z^2(r)]^{1/2} - a, \qquad [2.4]$$

where the surface profile is given by the function $z(r)$ as shown in Fig. 3. For a general surface profile the free energy F can be written as

$$F = 2\pi \int_0^\infty dr\, r\left[\gamma(1+z'^2)^{1/2} + E(D(r,z)) + \frac{1}{2}\Delta\rho g\left(z_o^\infty - z\right)^2\right]$$
$$+ \text{shape-independent terms}. \qquad [2.5]$$

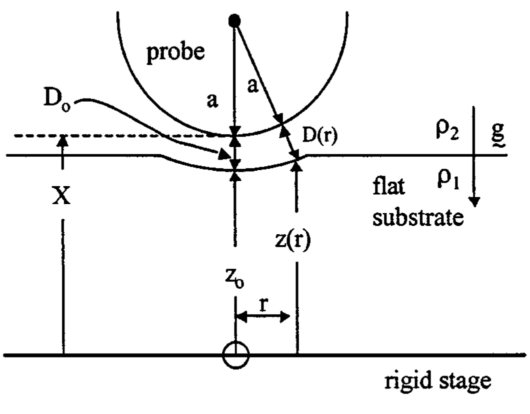

FIG. 3. Geometry of the rigid spherical probe at a flat liquid interface in the presence of gravity. (The deformation is not shown to scale.)

Here we use the Derjaguin approximation (10) for the interaction energy between the surfaces so that $E(D)$ is the interaction energy per unit area between parallel flat half spaces of probe and substrate material across a distance D of bathing medium. Minimizing the free energy with respect to drop shape (11), we obtain the augmented Young-Laplace equation

$$\gamma \frac{d}{dr}\left[\frac{z'r}{(1+z'^2)^{1/2}}\right] - r\,\Pi(D(r)) + r\,\Delta\rho g\left(z_o^\infty - z\right) = 0$$
$$(0 < r < \infty) \qquad [2.6]$$

and the boundary condition

$$z'(0) = 0. \qquad [2.7]$$

In deriving [2.6] we use the constraint that

$$z(\infty) = z_o^\infty \qquad [2.8]$$

together with the approximation that

$$\frac{\partial D(r,z)}{\partial z} = \frac{z - X - a}{a + D}$$
$$\approx -1 + O(D_o/a) \qquad [2.9]$$

and the definition of disjoining pressure as

$$\Pi(D) = -\frac{\partial E(D)}{\partial D}. \qquad [2.10]$$

Hence we have limited ourselves to the regime $D_o \ll a$ from the outset. The fact that $\partial D/\partial z$ is not -1 for $r \sim a$ is not of consequence since, in the derivation, it occurs multiplied by $\Pi(D(r))$ which will be vanishingly small by the time r achieves any small fraction of the sphere radius a. In the region where $\Pi(D)$ is not negligible, [2.9] is accurate to $O(D_o/a)$. That this is so is easily seen from the fact that we are interested in D_o values of order the decay length of the disjoining pressure $\Pi(D)$. Hence we expect that

$$z(r) - z_o \sim O(D_o) \qquad [2.11]$$

in the deformed region and we see from (2.1) and (2.4) that

$$r^2 = 2a[D(r) - D_o + z - z_o]\left(1 + O\left(\frac{D_o}{a}\right)\right). \qquad [2.12]$$

Thus the radial extent of the deformed region is $O((aD_o)^{1/2}) \ll a$. It follows that Fig. 3 is not shown strictly to scale, the deformation being over a very small section of the interface well inside $r \sim a$. The analysis below is therefore limited to lateral surface deformations which are small compared to the probe radius. In the case of “wrapping” (see Section 5) deformation of the interface may become comparable to probe radius and a more complicated treatment is necessary here.

Equation [2.6] is simply the Young-Laplace equation for a liquid interface under gravity in the presence of a disjoining pressure. Physically it is a statement that the local pressure difference across the interface (the Laplace (curvature) component plus the disjoining pressure) is equal to the pressure difference due to the gravitational head $z_o^\infty - z$. It is convenient to rearrange the equation as follows

$$z'' + \frac{1}{r}z' - (1+z'^2)^{3/2}\frac{\Pi(D)}{\gamma} + \frac{1}{\lambda^2}(1+z'^2)^{3/2}\left(z_o^\infty - z\right) + \frac{1}{r}z'^3 = 0, \qquad [2.13]$$

where we introduce the capillary length [1.10]. We solve this equation by matching inner ($r \sim (D_o a)^{1/2}$) and outer ($r \sim a$) solutions. To obtain the inner solution we write

$$r = (aD_o)^{1/2}t \qquad [2.14]$$

$$z - z_o = D_o\xi(t) \qquad [2.15]$$

so that

$$D(t) = D_o\left(1 - \xi + \frac{t^2}{2} + O(D_o/a)\right). \qquad [2.16]$$

Substituting these scalings into [2.13] we obtain

$$\xi'' + \frac{1}{t}\xi' - \frac{a\Pi(D_o(1-\xi+t^2/2))}{\gamma} = 0 + O(D_o/a) \qquad [2.17]$$

subject to

$$\xi'(0) = 0 \qquad [2.18]$$

$$\xi(0) = 0 \qquad [2.19]$$

which follows directly from [2.7] and [2.15]. The inner DE is not analytically solvable for a general $\Pi(D)$ but its large t asymptotic form is readily extracted.

A first integral of [2.17] is

$$t\xi' = \frac{a}{\gamma}\int_0^t dt\, t\Pi(D(t)), \qquad [2.20]$$

where [2.18] is used to eliminate the constant of integration. A second integral is then

$$\xi(t) = \frac{a}{\gamma}\int_0^t \frac{dt'}{t'}\int_0^{t'} dt''\, t''\Pi(D(t'')) \qquad [2.21]$$

where we make use of [2.19]. For large t, $\Pi(D(t))$ restricts the integration range by vanishing. Thus for $t \gg 1$ (i.e., outside the range of $\Pi(D)$ but well inside the sphere radius)

$$\xi(t) \sim \frac{1}{D_o}[G(D_o)\ln t - H(D_o)], \qquad [2.22]$$

where

$$\left.\begin{aligned} G(D_o) &= \frac{aD_o}{\gamma}\int_0^\infty dt\, t\Pi(D_o(1+t^2/2-\xi)) \\ H(D_o) &= \frac{aD_o}{\gamma}\int_0^\infty dt\, t\ln t\,\Pi(D_o(1+t^2/2-\xi)). \end{aligned}\right\} \qquad [2.23]$$

In unscaled variables the outer behavior of the inner solution is

$$z(r) = z_o - H(D_o) + G(D_o)\ln\left(\frac{r}{(aD_o)^{1/2}}\right). \qquad [2.24]$$

We note in passing that the total force on the interface is (in the Derjaguin approximation)

$$F(D_o) = 2\pi\int_0^\infty dr\, r\Pi(D(r)) \qquad [2.25]$$

$$= 2\pi\gamma G(D_o). \qquad [2.26]$$

The outer solution is scaled as

$$r = \lambda s \qquad [2.27]$$

$$z - z_o^\infty = a\chi(s). \qquad [2.28]$$

Here $\Pi(D)$ is negligible and Eq. [2.13] reduces to

$$\chi'' + \frac{1}{s}\chi' - \chi = 0 + O\left(\left(\frac{a}{\lambda}\right)^2\right) \qquad [2.29]$$

with

$$\chi, \chi' \xrightarrow[s\to\infty]{} 0. \qquad [2.30]$$

A suitable solution is

$$\chi(s) = -AK_o(s), \qquad [2.31]$$

where K_o is the modified Bessel function of the second kind (12). In unscaled variables the outer solution can be written

$$z(r) = z_o^\infty - aAK_o(r/\lambda). \qquad [2.32]$$

For small values of its argument (12)

$$K_o(z) \sim -\ln\frac{z}{2} - \mathrm{C} + O(z^2\ln z), \qquad [2.33]$$

where C = 0.57721566 is Euler's constant. Thus the inner asymptote of the outer solution is

$$
\begin{aligned}
z(r) &= z_o^\infty + aA[\ln(r/2\lambda) + \mathrm{C}] + \cdots \\
&= z_o^\infty + aA\ln\left(r/(D_o a)^{1/2}\right) - aA\ln\frac{2\lambda}{(D_o a)^{1/2}} + aA\mathrm{C}.
\end{aligned}
\tag{2.34}
$$

Comparison of [2.34] and [2.24] show that

$$aA = G(D_o) \tag{2.35}$$

and

$$z_o - H(D_o) = z_o^\infty - aA\ln\left(\frac{2\lambda}{(D_o a)^{1/2}}\right) + aA\mathrm{C}. \tag{2.36}$$

Hence

$$z_o = z_o^\infty + H(D_o) - G(D_o)\left(\ln\left(\frac{2\lambda}{(D_o a)^{1/2}}\right) - \mathrm{C}\right). \tag{2.37}$$

In terms of the AFM observable

$$X(D_o) = X_\infty + D_o + H(D_o) + G(D_o)\left[\mathrm{C} - \ln\frac{2\lambda}{(D_o a)^{1/2}}\right], \tag{2.38}$$

where

$$X_\infty = z_o^\infty. \tag{2.39}$$

For computational convenience, we use [2.16] to rewrite the inner differential equation [2.17] as

$$D'' + \frac{1}{t}D' - \left(2 - \frac{a\Pi(D)}{\gamma}\right)D_o = 0. \tag{2.40}$$

For the spherical drop/bubble case with a finite radius, R_o, and contact angle, θ_c, a similar analysis is employed and is presented in the appendix. The differential equation for the inner profile of the drop/bubble case is expressed in terms of $D(t)$ is (from [A.3] and [2.12])

$$D'' + \frac{1}{t}D' - \left(2\left(1 + \frac{a}{R_o}\right) - \frac{a\Pi(D)}{\gamma}\right)D_o = 0 \tag{2.41}$$

so that it reduces to the planar case when $a/R_o \ll 1$. Indeed, we note on comparison of the flat interface result [2.37] with the drop case [A.58] that, in both cases,

$$X(D_o) = X_\infty + D_o + H(D_o) + G(D_o)(1/2\ln D_o + B), \tag{2.42}$$

where B is a constant depending on the properties of the isolated interface, viz.

$$
\left.
\begin{aligned}
B_\infty &= \mathrm{C} + \ln\left(\frac{a^{1/2}}{2\lambda}\right) \\
B_{R_o} &= \mathrm{P}(\theta_c) + \ln\left(\frac{a^{1/2}}{2R_o}\right)
\end{aligned}
\right\}
\tag{2.43}
$$

while X_∞ $(= z_o^\infty)$ is the height of the undistorted interface at the center.

The theoretical calculation of $F(X)$, the observable result of an AFM experiment, is performed as follows. For a given function $\Pi(D)$, we solve [2.40] (or [2.41]) from $t = 0$ where $D(0) = D_o$ and $D'(0) = 0$ toward infinity evaluating the integrals

$$
\left.
\begin{aligned}
G &= \frac{aD_o}{\gamma}\int_0^t dt\, t\,\Pi(D(t)) \\
H &= \frac{aD_o}{\gamma}\int_0^t dt\, t\ln t\,\Pi(D(t))
\end{aligned}
\right\}
\tag{2.44}
$$

as we solve, until G and H have converged to $G(D_o)$ and $H(D_o)$ to within a specified accuracy. The force $F(D_o)$ is given by [2.26] and the distance $X(D_o)$ is given by [2.42]. Thus as D_o is varied systematically, we may plot $F(X)$ parametric in D_o. We show the results of those calculations for some model probe/drop systems in Section 3.

3. MODEL CALCULATIONS

We have chosen to illustrate the $F(X)$ behavior of a drop/probe system by using the electrostatic disjoining pressure alone. We have not included an attractive term as the treatment of systems where $\Pi(D)$ has an attractive component will be discussed in a subsequent paper where the interfacial instability will be treated. The disjoining pressure is calculated from the numerical solution of the full Poisson-Boltzmann equation between flats for 1 : 1 electrolyte with constant charge boundary conditions. The probe particle radius was set at 2 μm and the drop radius R_o at 0.5 mm. The calculation of $F(D_o)$ and $X(D_o)$ was performed by the algorithm discussed above for various values of the drop contact angle θ_c, the interfacial tension γ, surface potentials at infinite separation $\psi_{0_1}^\infty$, $\psi_{0_2}^\infty$ of probe and drop interfaces and double layer decay length, κ^{-1}.

In Figs. 4a and b we plot $F(D_o)/a$, $\Delta X(D_o)$ (i.e., $X(D_o) - X_\infty$) as functions of central separation D_o for $\psi_{0_1}^\infty = \psi_{0_2}^\infty =$ 50 mV, $\theta_c = 30^\circ$, $\gamma = 30$ dyn/cm. We note that both functions are strongly varying functions of D_o. Remarkably when F/a is plotted against ΔX (parametric in D_o) in Fig. 4c to produce the simulated AFM measurement, we observe the apparent onset of a linear compliance regime once $\Delta X(D_o)$ becomes negative (i.e., the bottom of the probe sphere is closer to the stage base than the top of the undistorted drop). In Fig. 5, we plot $F(\Delta X)/a$

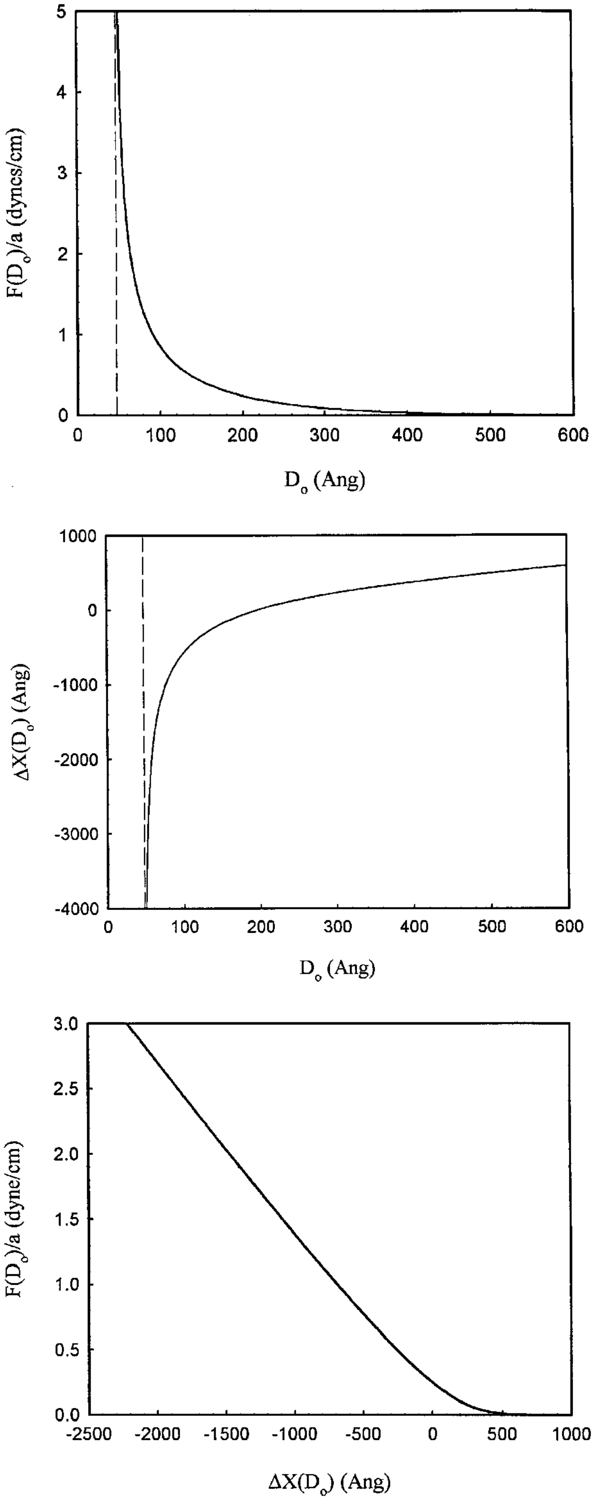

FIG. 4. $F(D_o)/a$ as a function of central separation distance, D_o, for $\psi_{0_1}^{\infty} = \psi_{0_2}^{\infty} = 50$ mV, $\theta_c = 30°$, $\gamma = 30$ dyn/cm, $\kappa^{-1} = 100$ Å, and $a = 2$ μm. The dashed vertical line denotes the wrapping distance, D_w. (b) $\Delta X(D_o)$ (i.e., $X(D_o) - X_\infty$) as a function of central separation distance, D_o, for $\psi_{0_1}^{\infty} = \psi_{0_2}^{\infty} = 50$ mV, $\theta_c = 30°$, $\gamma = 30$ dyn/cm, $\kappa^{-1} = 100$ Å, and $a = 2$ μm. The dashed vertical line denotes the wrapping distance, D_w. (c) $F(D_o)/a$ and $\Delta X(D_o)$ plotted parametrically as a function of central separation distance, D_o, for $\psi_{0_1}^{\infty} = \psi_{0_2}^{\infty} = 50$ mV, $\theta_c = 30°$, $\gamma = 30$ dyn/cm, $\kappa^{-1} = 100$ Å, and $a = 2$ μm.

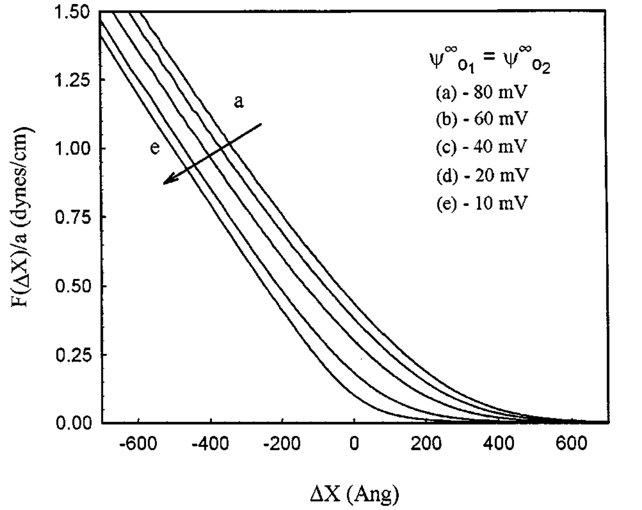

FIG. 5. $F(\Delta X)/a$ as a function of ΔX showing the effect of changing surface potential with system parameters $\theta_c = 30°$, $\gamma = 50$ dyn/cm, $\kappa^{-1} = 100$ Å, and $a = 2$ μm.

curves showing the effect of changing surface potential for interacting similar surfaces. Clearly the linear regime is a feature at all surface potentials. The slope of the linear compliance region is independent of ψ_o. The curves exhibit the asymptotic saturation behavior at large surface potentials that is a feature of electrostatic $\Pi(D)$'s calculated from the full nonlinear P-B equation.

In Fig. 6, we plot $F(\Delta X)/a$ for similar interacting surfaces with $\psi_{0_1}^{\infty} = \psi_{0_2}^{\infty} = 50$ mV, $\gamma = 50$ dyn/cm, and $\theta_c = 30°$ for various values of the Debye screening length κ^{-1}. We note the slope of the linear compliance region depends weakly on κ^{-1}. In Fig. 7, we plot $F(\Delta X)/a$ curves for $\psi_{0_1}^{\infty} = \psi_{0_2}^{\infty} = 50$ mV and $\gamma = 50$ dyn/cm for various values of the drop contact angle θ_c. Again we note the linear compliance region and a moderately

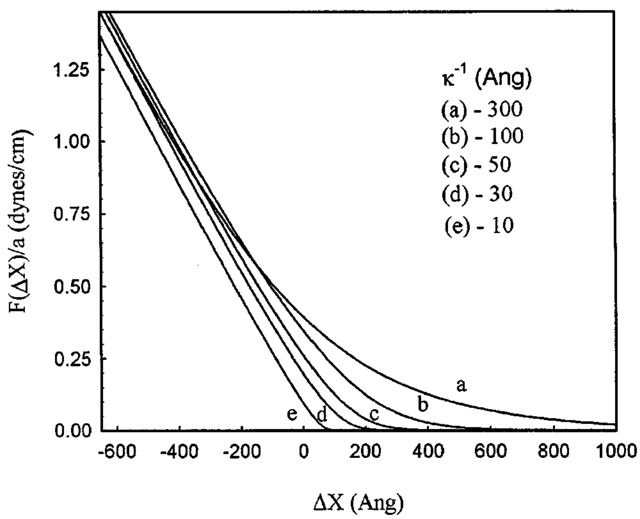

FIG. 6. $F(\Delta X)/a$ as a function of ΔX for various values of the Debye screening length κ^{-1} with system parameters $\psi_{0_1}^{\infty} = \psi_{0_2}^{\infty} = 50$ mV, $\theta_c = 30°$, $\gamma = 50$ dyn/cm, and $a = 2$ μm.

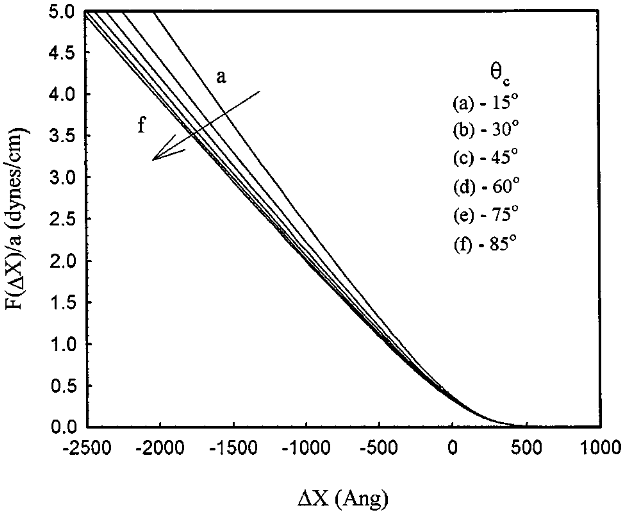

FIG. 7. $F(\Delta X)/a$ as a function of ΔX for various values of the drop contact angle θ_c with system parameters $\psi_{0_1}^{\infty} = \psi_{0_2}^{\infty} = 50$ mV, $\kappa^{-1} = 100$ Å, $\gamma = 50$ dyn/cm, and $a = 2$ μm.

strong dependence of the compliance (slope) on contact angle. In Fig. 8, we plot $F(\Delta X)/a$ curves for dissimilar interacting surfaces with surface potentials $\psi_{0_1}^{\infty}$ and $\psi_{0_2}^{\infty}$ as shown for $\theta_c = 30°$ and $\gamma = 50$ dyn/cm. The disjoining pressure $\Pi(D)$ for dissimilar surfaces has more structure than in the similar surfaces case and cannot be well approximated at smaller separations by a single exponential decay as it can at larger separations. Nevertheless, the linear compliance region still manifests itself as a weak function of surface potentials. Clearly linear compliance is not associated just with approximately exponential force laws. Finally in Fig. 9 we plot $F(\Delta X)/2\pi\gamma a$ as a function of ΔX for $\psi_{0_1}^{\infty} = \psi_{0_2}^{\infty} = 50$ mV, $\theta_c = 30°$, and various values of γ and we note a very weak residual dependence of the compliance on

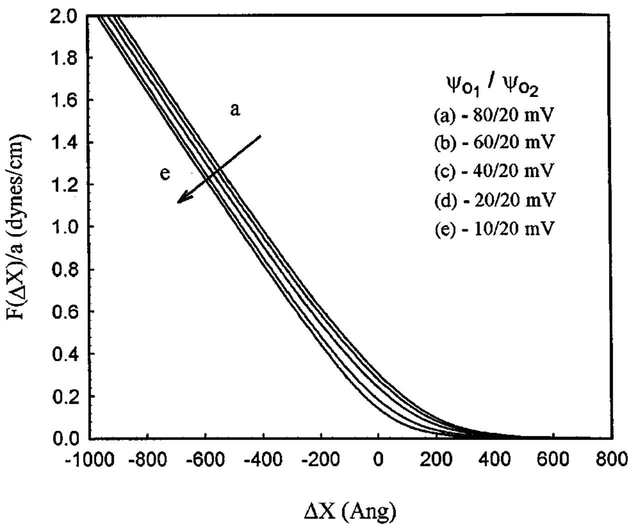

FIG. 8. $F(\Delta X)/a$ as a function of ΔX for dissimilar interacting surfaces with surface potentials $\psi_{0_1}^{\infty}$ and $\psi_{0_2}^{\infty}$ for $\kappa^{-1} = 100$, $\theta_c = 30°$, $\gamma = 50$ dyn/cm, and $a = 2$ μm.

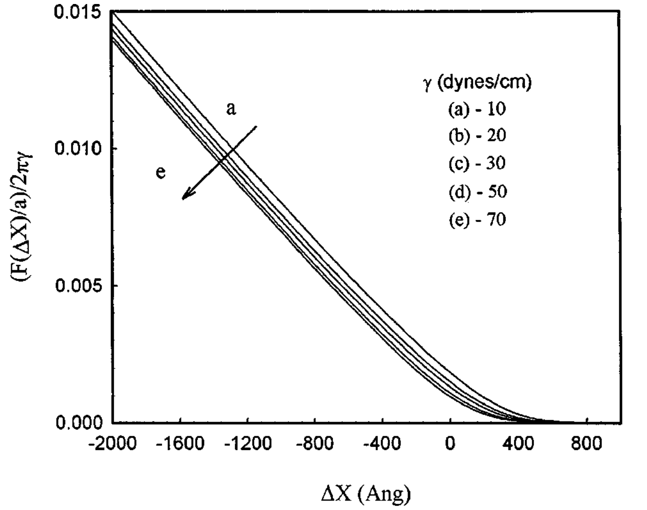

FIG. 9. $F(\Delta X)/2\pi\gamma a$ as a function of ΔX for various values of γ with system parameters $\psi_{0_1}^{\infty} = \psi_{0_2}^{\infty} = 50$ mV, $\kappa^{-1} = 100$ Å, $\theta_c = 30°$, and $a = 2$ μm.

surface tension over and above the explicit linear dependence which we removed by plotting $F/(2\Pi\gamma a)$.

4. THE DROP AS A HOOKEAN SPRING

We test here the assumption that the distorted drop/bubble behaves mechanically as a Hookean spring. We see from [1.7] and the definition [2.1] of $X(D_o)$ that we wish to test the hypothesis that

$$F(D_o) = -K(\Delta X(D_o) - D_o), \qquad [4.1]$$

where K is a constant for all D_o values. We note that the point $\Delta X - D_o = 0$ corresponds to infinite separation of drop and probe. At large separation the disjoining pressure (along with $G(D_o)$ and $H(D_o)$) vanishes and $\Delta X \sim D_o$. In Fig. 10, we replot

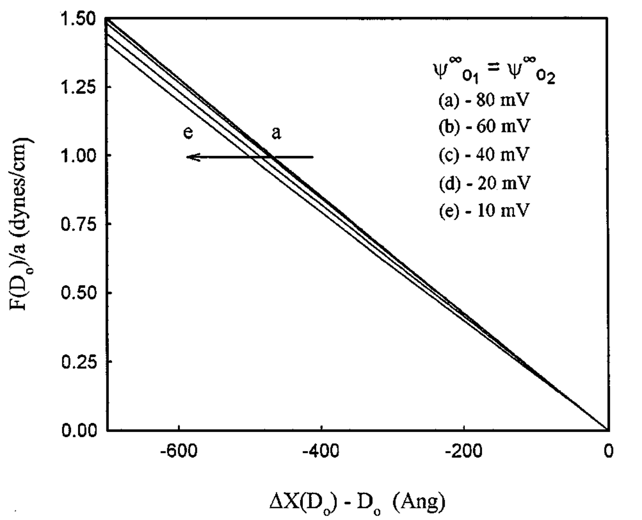

FIG. 10. Replot the curves of Fig. 5 showing the effect of changing surface potential as F/a versus $\Delta X - D_o$.

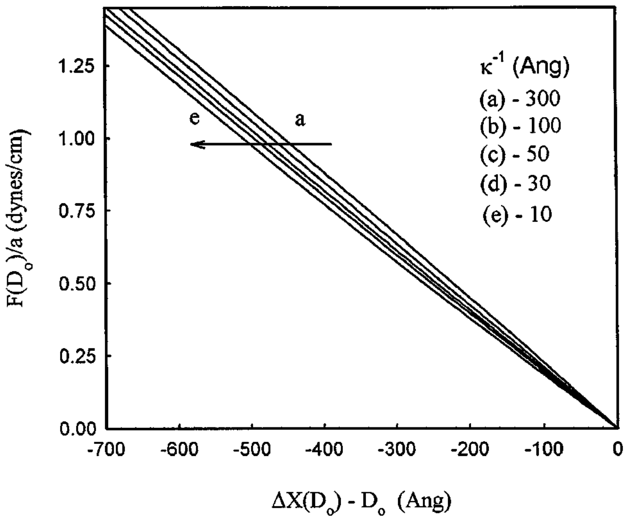

FIG. 11. Replot the curves of Fig. 6 for various κ^{-1} values as F/a versus $\Delta X - D_o$.

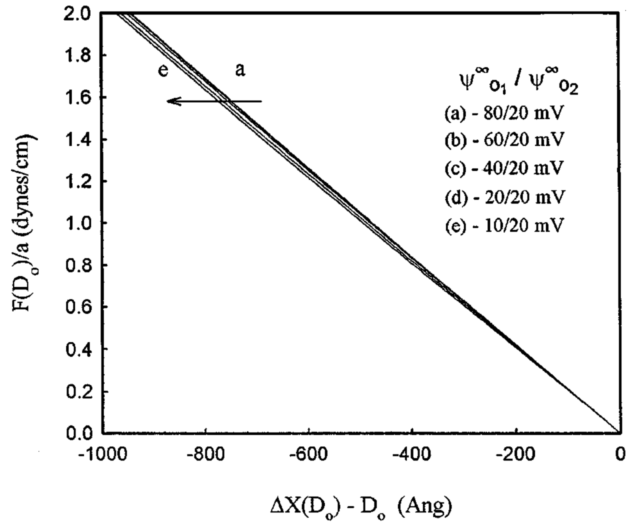

FIG. 13. Replot the curves of Fig. 8 for dissimilar surface potentials as F/a versus $\Delta X - D_o$.

the curves of Fig. 5 as F/a versus $\Delta X - D_o$. The curves for lower surface potentials show a weak dependence on surface potential while curves for higher surface potentials collapse into a single curve over most of their length. Again this behavior is indicative of the asymptotic saturation at higher surface potentials for electrostatic force laws as discussed in Section 3. In Fig. 11, we replot the curves of Fig. 6 for various κ^{-1} values against $\Delta X - D_o$. The moderate dependence of the compliance on κ^{-1} should be noted. In Fig. 12 we replot the curves of Fig. 7 for various contact angles θ_c as a function of $\Delta X - D_o$. There is again the strong dependence of compliance on θ_c. In Fig. 13, we replot the curves of Fig. 8 for dissimilar surface potentials as functions of $\Delta X - D_o$ and we note a similar behavior as in Fig. 10. In Fig. 14, we replot the $F(\Delta X)/2\pi\gamma a$ curves of Fig. 9 (where γ was varied) as functions of the distortion $\Delta X - D_o$ and note the marked insensitivity to the value of γ even though the linear region of $F(\Delta X)$ in Fig. 9 does exhibit a moderate dependence.

We note from these plots that a Hookean force law is valid for low to moderate distortions with perhaps a slight strengthening of the spring constant as distortion becomes large. As stated above the present theory is restricted to lateral deformation of the order $(aD_o)^{1/2}$. We note the dependence of the spring constant on contact angle θ_c and the range κ^{-1} of the disjoining pressure, and the linear dependence on interfacial tension γ. The spring constant appears to be insensitive to the magnitude of the disjoining pressure for higher surface potentials. In the next section, we develop a tentative theory for the Hookean response of a drop, which goes some way toward explaining and quantifying these features.

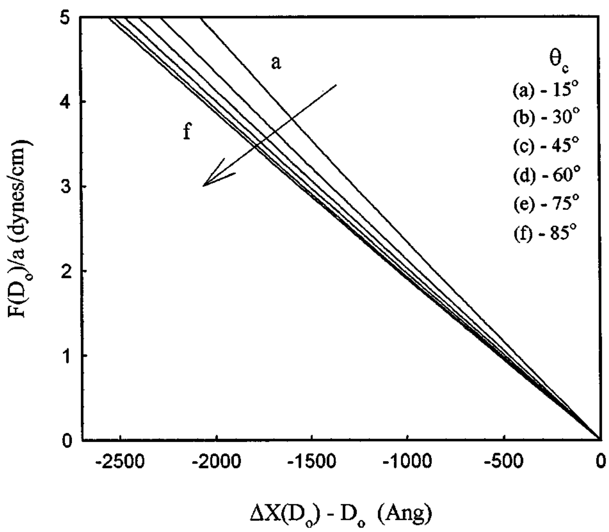

FIG. 12. Replot the curves of Fig. 7 for various contact angles θ_c as F/a versus $\Delta X - D_o$.

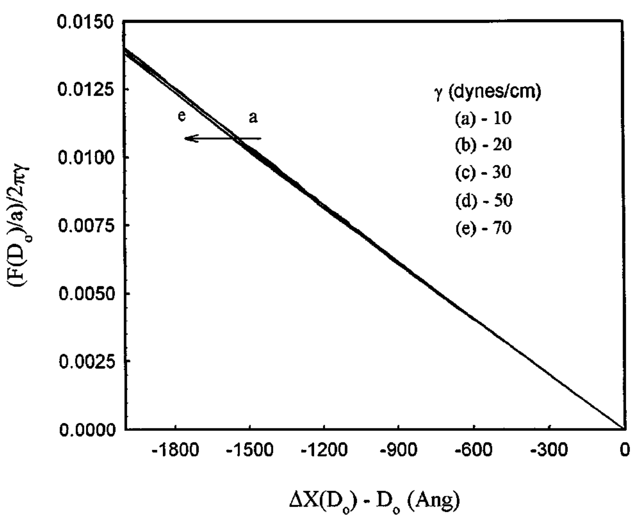

FIG. 14. Replot the $F(\Delta X)/2\pi\gamma a$ curves of Fig. 9 for various values of γ as F/a versus $\Delta X - D_o$.

5. THE DISJOINING PRESSURE ORIGIN OF LINEAR COMPLIANCE

Useful light may be shed on origins of the linear compliance by a rescaling of the inner profile equation [2.41]. We introduce the variable

$$x = D_o^{1/2}\left[-\frac{\partial \ln \Pi}{\partial D}\bigg|_{D_o}\right]^{1/2} t \qquad [5.1]$$

$$= \frac{r}{\left(a\left[-\frac{\partial \ln \Pi}{\partial D}\big|_{D_o}\right]^{-1}\right)^{1/2}} \qquad [5.2]$$

which amounts to using the true range of the disjoining pressure instead of D_o in the scaling of the radial distance r. With this scaling

$$G(D_o) = \frac{a}{\gamma\left(-\frac{\partial \ln \Pi}{\partial D}\big|_{D_o}\right)} \int_0^x dx\, x \Pi(D(x)) \qquad [5.3]$$

$$H(D_o) = G(D_o)\left[-\frac{1}{2}\ln D_o - \frac{1}{2}\ln\left(-\frac{\partial \ln \Pi}{\partial D}\bigg|_{D_o}\right) + \frac{\int_0^x dx\, x \ln x \Pi(D(x))}{\int_0^x dx\, x \Pi(D(x))}\right] \qquad [5.4]$$

so that from [2.42]

$$X(D_o) = X_\infty + D_o + G(D_o)\left[B - \frac{1}{2}\ln\left(-\frac{\partial \ln \Pi}{\partial D}\bigg|_{D_o}\right) + \frac{\int_0^x dx\, x \ln x \Pi(D(x))}{\int_0^x dx\, x \Pi(D(x))}\right]. \qquad [5.5]$$

We may therefore write (using [2.26])

$$F(D_o) = -K(D_o)[X(D_o) - X_\infty - D_o], \qquad [5.6]$$

where

$$\frac{2\pi\gamma}{K(D_o)} = -B + \frac{1}{2}\ln\left(-\frac{\partial \ln \Pi}{\partial D}\bigg|_{D_o}\right) - \frac{\int_0^x dx\, x \ln x \Pi(D(x))}{\int_0^x dx\, x \Pi(D(x))}. \qquad [5.7]$$

This is an exact result, which suggests (but does not prove) that a linear compliance region exists provided $\Delta X(D_o) \gg D_o$ and that the system is Hookean. To prove this we must be able to argue that $K(D_o)$ is sensibly a constant. We know from the numerical results of the previous section that such an argument must be able to be made in view of the linearity of the Hookean plots under a fairly broad range of conditions for small to moderate deformations.

Since the second and third terms in [5.7] are already insensitive to the magnitude of $\Pi(D_o)$ the observation of insensitivity of the effective spring constant of the drop to the surface potential is immediately explained. The second term varies logarithmically with the range of the disjoining pressure and may well explain the observed weak dependence on κ^{-1}. It is clear from [5.7] that the contact angle dependence is contained solely and explicitly in the B term since the second and third terms are independent of the particulars of the outer solution. We note that the third term retains a dependence on surface tension since $D(t)$ satisfies a differential equation ([2.40] or [2.41]) which explicitly contains γ but from the numerical results of Section 4, the γ dependence of the third term must be very weak.

It is clear from the inner equation for the drop profiles, Eq. [2.41], that when $D_o = D_w$ where the wrapping distance is defined by

$$\Pi(D_w) = 2\gamma\left(\frac{1}{a} + \frac{1}{R_o}\right) \qquad [5.8]$$

the solution $D(t)$ is

$$D(t) = D_w \quad (0 < t < \infty) \qquad [5.9]$$

and

$$G(D_w) = H(D_w) = \infty. \qquad [5.10]$$

For constant charge interactions where $\Pi(D)$ diverges as $D \to 0$ a wrapping distance D_w will always exist. For low potentials and high surface tensions, the D_w value for constant charge interaction will be small. If the disjoining pressure scales as γ/D_o ($\gg 2\gamma/a$) (as is the case for dispersion forces), then the wrapping distance could be at a considerable separation distance just as the disjoining pressure begins to rise. For dissimilar surfaces under constant potential, there is a maximum repulsive electrostatic pressure and ultimate attraction. This sort of $\Pi(D)$ curve can also be achieved by adding an attractive interaction (as in classical DLVO theory) which ultimately dominates the total interaction. The present analysis is applicable to these systems only up to the D_o values of the maximum repulsive pressure (see Fig. 8). For smaller D_o values, these sorts of disjoining pressures require a an additional treatment to monitor for the cantilever and interfacial instabilities, which are inherent. Such cases will be discussed in detail in a subsequent publication.

We note in passing that the addition of ionic surfactant to the probe/oil drop system has a twofold mechanism for encouraging wrapping to occur. It enhances both interfacial surface potentials and tends to make them equal (i.e., $\Pi(D)$ for similar surfaces $> \Pi(D)$ for dissimilar surfaces) and it lowers the surface tension of the drop.

We see that D_w is a parameter that can range widely depending on the nature of the disjoining pressure function $\Pi(D)$. Physically the wrapping distance is such that the repulsive

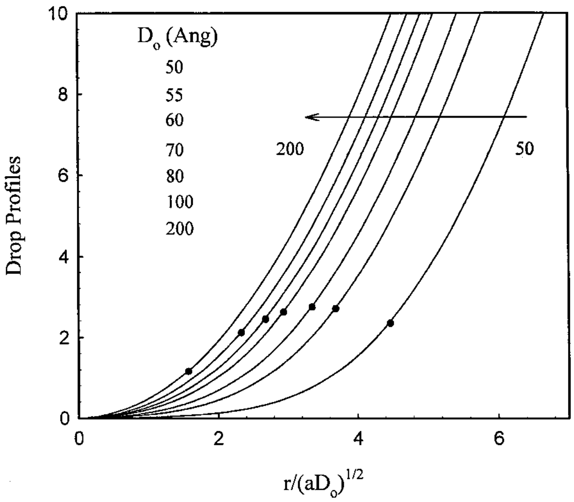

FIG. 15. Drop profiles, $(D(t) - D_o)/D_o$, as a function of dimensionless radial distance, $r/\sqrt{aD_o}$, for the calculations pertaining to Fig. 4 for various D_o values. $D(t)$ was calculated by solving the ordinary differential equation given in Eq. [3.54]. The dots denote the point at which G (Eq. [2.44]) is equal to 90% of its limiting value $G(D_o)$ for each D_o value.

disjoining pressure is large enough to cancel the Laplace pressure difference $2\gamma/R_o$ of the undistorted drop and then to bend the interface in the opposite direction with an additional pressure $\frac{2\gamma}{(a+D_w)} = \frac{2\gamma}{a}(1 + O(D_w/a))$ so that the liquid interface conforms to the shape of the probe particle. In Figs. 4a and b we mark the wrapping distance D_w that pertains to that disjoining pressure, surface tension, and sphere radius. Clearly the linear compliance region has set in for D_o values much larger than D_w. This is a feature common to all cases examined. So the onset of wrapping is not the origin of the linearity assumed in the conventional renormalization of AFM measurements and discussed in Section 1 above. *Linear compliance does not imply constant compliance* ($D_o = D_w$).

Nevertheless, the concept that, as D_o decreases, the drop profile flattens and then inverts (with $D(t)$ becoming flatter and the flattened region extending further from the center) is the root cause of the linearity. In Fig. 15 we show drop profiles, $(D(t) - D_o)/D_o$, for the calculations pertaining to Fig. 4 for various D_o values, which clearly illustrates the effect for a typical repulsive disjoining pressure. It follows that, as the profile flattens, the contributions to the $G(D_o)$, $H(D_o)$ integrals from the flattened region $D \sim D_o$ are becoming dominant. This is illustrated in Fig. 15 where we mark the position along each curve at which G (Eq. [2.44]) is equal to 90% of its limiting value $G(D_o)$. This observation suggests a variety of approximate methods for evaluating the third term of Eq. [5.7] for the drop "spring constant." We will not pursue this matter further here.

6. IMPLICATIONS FOR THE AFM MEASUREMENT

We have demonstrated numerically and analytically that the drop/probe system behaves as a Hookean spring for small and moderate central deformations of the drop so that Eq. [1.7] for D_o is valid in this regime. As we have demonstrated D_o is not constant in the apparent linear compliance region but, experimentally l and l_∞ are substantially greater than D_o in this regime so that D_o can be neglected in Eq. [1.7] to produce the linear compliance equation.

$$d = \left(1 + \frac{K_c}{K_d}\right)^{-1}(l - l_\infty). \qquad [6.1]$$

The intercept l_∞ determined from the linear compliance region will be systematically inaccurate by an amount of order the D_o values pertaining to that region. Having obtained a value of $1 + K_c/K_d$ and l_∞ we could use [1.7] to obtain D_o values outside the constant compliance regime but they would be too small by the amount that l_∞ is in error.

If one examines the $F(\Delta X)$ curves calculated in Section 4 above, it will be noted that the linear compliance region does not intercept the ΔX axis at the origin but at a distance on the positive side comparable to the D_o values pertaining to the linear compliance region. This is precisely the systematic error we cannot avoid in attempting to renormalize the AFM measurements to obtain absolute D_o values. Equation [1.7] is not useful except at very large D_o values where the error would be relatively small. The Ducker equation [1.9] exhibits a similar problem in that D_w is not known *a priori* and it is not negligible. Of course, [1.9] should not be used to obtain D_o since we have demonstrated that D_o can be substantially larger than D_w and is varying over the linear compliance region.

It is our opinion that the best that can be done is to measure $F(X)$. Any attempt to obtain D_o values must be made in the manner outlined in this paper, viz. assume a parameterized $\Pi(D)$ form and calculate a theoretical $F(X)$ curve which can be fitted to the measured curve to obtain the best fit parameter values. The D_o values are obtained in the course of that calculation. We will examine such a fitting procedure in a future publication.

APPENDIX

The geometry of the probe/drop case is shown in Fig. A.1. Here we assume the drop (bubble) in isolation has a spherical shape with radius of curvature R_o and a radial extent on the stage r_1. We assume $a < R_o \ll \lambda$ so that gravity may be neglected. As the probe is pressed into the drop, the drop will bulge by a very small amount. We assume that the contact line does not move during this displacement so that r_1 is fixed. The existence of finite contact angle hysteresis for experimental systems will ensure this. The free energy is now

$$F = 2\pi \int_0^{r_1} dr\, r\left[\gamma(1 + z'^2)^{1/2} + E(D(r, z))\right]$$
$$+ \text{shape-independent terms.} \qquad [A.1]$$

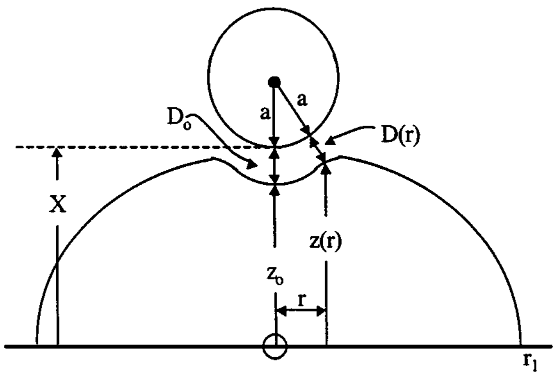

FIG. A1. The geometry of the probe/drop experiment. The drop has an undistorted radius of curvature, R_o, such that $a \ll R_o \ll \lambda$ so that gravitational distortion can be neglected. (The deformation is not shown to scale.)

To obtain the drop shape equation, we minimize F with respect to $z(r)$ as previously, but we must now constrain the variation with the constancy of the drop volume

$$V = 2\pi \left[\int_0^{R_+} dr\, rz - \int_{r_1}^{R_+} dr\, rz \right], \qquad [A.2]$$

where R_+ is the maximum radial extent of the drop [A.32]. Introducing the undetermined multiplier Λ and minimizing $F - \Lambda V$ we obtain (11)

$$\pm\gamma \frac{d}{dr}\left(\frac{z'r}{(1+z'^2)^{1/2}}\right) - r\Pi(D) = -\Lambda r \qquad [A.3]$$

and the trivial boundary condition

$$z'(0) = 0. \qquad [A.4]$$

The upper sign in [A.3] pertains for a drop which makes an acute contact angle with the substrate. For obtuse contact angles the upper sign pertains to the upper part of the drop and the lower sign to the lower part between the contact point $r = r_1$ and the maximum radius $r = R_+$ (see [A.32]). Again we have made the approximations ($D_o/a \ll 1$) discussed in the previous section in deriving [A.2]. Physically, [A.3] asserts that the local pressure difference (Laplace pressure + disjoining pressure) should be a constant everywhere on the interface—the constant, of course, being the difference in internal and external liquid pressures. For convenience we write the parameter Λ as

$$\Lambda = \frac{2\gamma}{R}, \qquad [A.5]$$

where the constant R is very close to the undistorted radius R_o but the difference is important as discussed below. R does not have a geometric interpretation on Fig. 4. A first integral of [A.3] using [A.4] is

$$\pm\frac{z'r}{(1+z'^2)^{1/2}} = -\frac{r^2}{R} + \Gamma(r), \qquad [A.6]$$

where

$$\Gamma(r) = \frac{1}{\gamma}\int_0^r dr\, r\Pi(D(r)). \qquad [A.7]$$

Rearranging [1.10] we obtain

$$z' = \frac{\pm(-r^2/R + \Gamma(r))}{\{r^2 - (-r^2/R + \Gamma(r))^2\}^{1/2}}. \qquad [A.8]$$

Equation [A.8] is the start of the process of generating inner and outer solutions for matching purposes. With the usual inner scaling [2.14], [2.15], and [2.16] the inner differential equation becomes

$$\xi' = -\frac{a}{R}t + \frac{\Gamma(t)}{D_o t} + O\left(\frac{D_o}{R}\right), \qquad [A.9]$$

where we regard Γ/D_o as, at least, an $O(1)$ quantity. To see why, we write [A.7] as

$$\frac{\Gamma(t)}{D_o} = \frac{a}{\gamma}\int_0^{(aD_o)^{1/2}t} dt\, t\Pi(D(t)). \qquad [A.10]$$

The disjoining pressure scales as

$$\Pi(D) \sim \frac{\gamma}{D_o} f(D/D_o) \qquad [A.11]$$

so that

$$\frac{\Gamma(t)}{D_o} \sim \frac{a}{D_o}\int_0^{(aD_o)^{1/2}t} dt\, t f(D(t)/D_o). \qquad [A.12]$$

Thus how large $\Gamma(t)/D_o$ can be will depend on the value of $f(1)$ which for some D_o values will be small.

A second integral of [2.7] using the boundary condition [2.19] yields

$$\begin{aligned}\xi(t) &= -\frac{a}{2R}t^2 + \frac{1}{D_o}\int_0^t \frac{dt}{t}\Gamma(t) \\ &= -\frac{a}{2R}t^2 + \frac{a}{\gamma}\int_0^t dt'\, t'\Pi(D(t'))(\ln t - \ln t') \end{aligned} \qquad [A.13]$$

with the aid of [2.15] and a change of order of integration. Thus we have, for large t,

$$\xi(t) = -\frac{a}{2R}t^2 - \frac{H(D_o)}{D_o} + \frac{G(D_o)}{D_o}\ln t + \cdots +, \qquad [A.14]$$

where $H(D_o)$ and $G(D_o)$ have been defined in Section 2. In unscaled variables, the outer form of the inner solution is

$$z(r) = z_o - \frac{r^2}{2R} - H(D_o) + G(D_o)\ln\left(\frac{r}{(aD_o)^{1/2}}\right) + \cdots + . \quad [A.15]$$

For the outer solution we adopt the scalings

$$r = (GR)^{1/2}s \quad z(r) = (GR)^{1/2}\chi(s) \quad [A.16]$$

and recognize the $\Gamma(r)$, in this distance regime, can be replaced by $\Gamma(\infty)$ which from [A.10] is simply $G(D_o)$ which we restrict here to positive values (predominately repulsive potentials). The profile equation becomes, for the outer region,

$$\chi' = \frac{\pm(1-s^2)}{(s_+^2 - s^2)^{1/2}(s^2 - s_-^2)^{1/2}}, \quad [A.17]$$

where

$$s_+^2 s_-^2 = 1 \quad [A.18]$$

$$s_+^2 + s_-^2 = \frac{R}{G} + 2 \quad [A.19]$$

with solution

$$\chi = \int_s^{s_+} \frac{ds(s^2-1)}{(s_+^2 - s^2)^{1/2}(s^2 - s_-^2)^{1/2}} \mp \int_{s_1}^{s_+} \frac{ds(s^2-1)}{(s_+^2 - s^2)^{1/2}(s^2 - s_-^2)^{1/2}}, \quad [A.20]$$

where

$$s_1 = r/(GR)^{1/2}(\gg 1). \quad [A.21]$$

In [A.20] the upper sign refers to acute drop profiles and the lower sign refers to obtuse drop profiles. Fortunately the integral [A.20] can be evaluated exactly in terms of the incomplete elliptic integrals (12) E and F. We have that

$$\chi(s) = s_+\mathrm{E}(\mathrm{K}(s), q) - \frac{1}{s_+}\mathrm{F}(\mathrm{K}(s), q) \mp \left(s_+\mathrm{E}(\mathrm{K}(s_1), q) - \frac{1}{s_+}\mathrm{F}(\mathrm{K}(s_1), q)\right) \quad [A.22]$$

where

$$\mathrm{K}(s) = \mathrm{Sin}^{-1}\left(\frac{s_+^2 - s^2}{s_+^2 - s_-^2}\right)^{1/2} \quad [A.23]$$

$$q^2 = 1 - \left(\frac{s_-}{s_+}\right)^2 \quad [A.24]$$

$$\mathrm{F}(\mathrm{K}, q) = s_+ \int_s^{s_+} \frac{ds}{(s_+^2 - s^2)^{1/2}(s^2 - s_-^2)^{1/2}} \quad [A.25]$$

$$\mathrm{E}(\mathrm{K}, q) = \frac{1}{s_+} \int_s^{s_+} \frac{ds\, s^2}{(s_+^2 - s^2)^{1/2}(s^2 - s_-^2)^{1/2}}. \quad [A.26]$$

To match this solution to the inner solution, we consider s in range $s_- \ll s \ll s_+$ (i.e., $G \ll r \ll R$). From [A.18] and [A.19] it follows that

$$s_+ = (R/G)^{1/2}(1 + G/R + \cdots) \quad [A.27]$$

$$s_- = (G/R)^{1/2}(1 - R/G + \cdots). \quad [A.28]$$

Hence

$$q^2 = 1 - O((G/R)^2) \quad [A.29]$$

$$\mathrm{Sin\ K}(s) = 1 - \frac{G}{2R}s^2(1 + O(G/R)) \quad [A.30]$$

$$\mathrm{Sin\ K}(s_1) = (1 - (r_1/R_+)^2)^{1/2}(1 + O(G/R)^2), \quad [A.31]$$

where

$$R_+ = (RG)^{1/2}s_+ = R + G + \cdots. \quad [A.32]$$

Note that for $q^2 \approx 1$ (12),

$$\mathrm{E}(\mathrm{K}, q) = \mathrm{Sin\ K} + \cdots \quad [A.33]$$

$$\mathrm{F}(\mathrm{K}, q) = \frac{1}{2}\ln\left(\frac{1 + \mathrm{Sin\ K}}{1 - \mathrm{Sin\ K}}\right) + \cdots. \quad [A.34]$$

Substitution of these limiting forms in the exact equation [A.22] yields

$$\chi(s) = \left(\frac{R}{G}\right)^{1/2}\left(1 + \frac{G}{R}\right)\left[1 - \frac{Gs^2}{2R} \mp \left(1 - \left(\frac{r_1}{R_+}\right)^2\right)^{1/2}\right] - \left(\frac{G}{R}\right)^{1/2}\left[-\frac{1}{2}\ln\left(\frac{Gs^2}{4R^2}\right) \mp \frac{1}{2}\ln\left(\frac{1 + (1 - (r_1/R_+)^2)^{1/2}}{1 - (1 - (r_1/R_+)^2)^{1/2}}\right)\right] + \cdots \quad [A.35]$$

which in unscaled variables can be written as

$$z(r) = R\left(1 \mp \left(1 - \left(\frac{r_1}{R_+}\right)^2\right)^{1/2} - \frac{r_2}{2R_2}\right) + G\left[\frac{1}{2}\ln\left(\frac{r^2}{4R^2}\right) \pm \frac{1}{2}\ln\left(\frac{1 + (1 - (r_1/R_+)^2)^{1/2}}{1 - (1 - (r_1/R_+)^2)^{1/2}}\right) + 1 \mp \left(1 - \left(\frac{r_1}{R_+}\right)^2\right)^{1/2}\right] + \cdots. \quad [A.36]$$

Comparison of this form with the inner solution [A.15] yields

$$\begin{aligned} z_o &= R(1 \mp (1-(r_1/R_+)^2)^{1/2}) + H(D_o) + G(D_o) \\ &\quad \times \left\{ \frac{1}{2}\ln\left(\frac{aD_o}{4R^2}\right) \pm \frac{1}{2}\ln\left[\frac{1+(1-(r_1/R)^2)^{1/2}}{1-(1-(r_1/R)^2)^{1/2}}\right] \right. \\ &\quad \left. + 1 \mp \left(1-\left(\frac{r_1}{R_+}\right)^2\right)^{1/2} \right\}. \end{aligned} \quad [A.37]$$

We now write

$$R_+ = R_o + \delta R + G \quad [A.38]$$

and use the fact that $\delta R/R_o$ is $O(G/R)$ to rewrite [A.37] as

$$\begin{aligned} z_o &= R_o(1 \mp (1-(r_1/R_o)^2)^{1/2}) \\ &\quad + \delta R\left[1 \mp \frac{1}{(1-(r_1/R_o)^2)^{1/2}}\right] + H(D_o) + G(D_o) \\ &\quad \times \left\{ \frac{1}{2}\ln\left(\frac{aD_o}{4R_o^2}\right) \pm \frac{1}{2}\ln\left(\frac{1+(1-(r_1/R_o)^2)^{1/2}}{1-(1-(r_1/R_o)^2)^{1/2}}\right) \right. \\ &\quad \left. + 1 \mp \frac{1}{(1-(r_1/R_o)^2)^{1/2}} \right\}, \end{aligned} \quad [A.39]$$

where we have neglected $O((G/R)^2)$ terms. In deriving [A.39] we have assumed that $1-(r_1/R_o)^2 \gg G/R_o$. This will not be valid for contact angles very close to $\pi/2$ (i.e., $r_1 = R_o$) and a separate analysis for this case would need to be made. Since the result which we will derive for contact angles such that $1-(r_1/R_o)^2 \gg G/R_o$ will be valid for $|\theta_c - \pi/2| \gg (G/R)$ and since this result does not diverge as $\theta_c \to \pi/2$ from above or below we do not examine this limit here.

The last three terms on the RHS of [A.36] are $O(D_o)$ terms. Clearly we need to calculate δR to complete the solution. The undetermined multiplier $2\gamma/R$ is determined *a postiori* by the volume constraint. By integration by parts [A.2] may be written as

$$V = V_O + V_I, \quad [A.40]$$

where

$$V_I = \int_0^{r_o} dr\, r^2 z' \quad [A.41]$$

and

$$V_O = -\pi\int_{r_o}^{R_+} dr\, r^2 z' + \pi\int_{r_1}^{R_+} dr\, r^2 z', \quad [A.42]$$

where r_o is a value of r in the matching region ($G \ll r_o < R$). In the region $0 < r < r_o$ z' is given by (from [A.9])

$$z' = -\frac{r}{R} + \frac{\Gamma(r)}{r} + \cdots \quad [A.43]$$

so that

$$\begin{aligned} V_I &= -\pi\int_0^{r_o} dr\, r\left(-\frac{r^2}{R} + \Gamma(r)\right) + \cdots \\ &= -\pi a D_o^2 \int_0^{r_o/(aD_o)^{1/2}} dt\, t\left(-\frac{a}{R}t^2 + \Gamma/D_o\right) \\ &= V\left(\frac{a}{R_o}\right) O((D_o/R_o)^2), \end{aligned} \quad [A.44]$$

where the drop volume V is $O(R_o^3)$. To calculate δR, the drop volume must be calculated to $O(D_o/R_o)$. It follows that V_I can be neglected to this order and hence (using the outer scaling [A.16])

$$\begin{aligned} V &= \pi(RG)^{3/2}\left[\int_{s_o}^{s_+} \frac{ds\, s^2(s^2-1)}{(s_+^2-s^2)^{1/2}(s^2-s_-^2)^{1/2}} \right. \\ &\quad \left. \pm \int_{s_1}^{s_+} \frac{ds\, s^2(s^2-1)}{(s_+^2-s^2)^{1/2}(s^2-s_-^2)^{1/2}}\right] + \cdots, \end{aligned} \quad [A.45]$$

where we use the outer form [A.17] for the scaled z'.

Performing the integrations we obtain

$$V = \pi(RG)^{3/2}[J(s_o) \mp J(s_1)], \quad [A.46]$$

where

$$\begin{aligned} J(s) &= \frac{s}{3}(s_+^2-s^2)^{1/2}(s^2-s_-^2)^{1/2} - \frac{1}{3s_+}\mathrm{F}(\mathrm{K}(s), q) \\ &\quad + \left(\frac{2R}{G}+1\right)\frac{s_+}{3}\mathrm{E}(\mathrm{K}(s), q). \end{aligned} \quad [A.47]$$

Using the limiting forms [A.29] to [A.34] we obtain

$$J(s_o) = \left(\frac{R}{G}\right)^{3/2}\left(\frac{2}{3} + \frac{G}{R} + O((G/R)^2)\right) \quad [A.48]$$

and

$$\begin{aligned} J(s_1) &= \left(\frac{R}{G}\right)^{3/2}\left(\frac{2}{3} + \frac{1}{3}\left(\frac{r_1}{R}\right)^2 + \frac{G}{R}\left(1+\frac{1}{3}\left(\frac{r_1}{R}\right)^2\right)\right. \\ &\quad \left. + O((G/R)^2)\right)\left(1-\left(\frac{r_1}{R_+}\right)^2\right)^{1/2}. \end{aligned} \quad [A.49]$$

Hence

$$\begin{aligned} V &= \pi R^3\left[\frac{2}{3} \mp \frac{1}{3}\left(2+\left(\frac{r_1}{R}\right)^2\right)\left(1-\left(\frac{r_1}{R_+}\right)^2\right)^{1/2} + \frac{G}{R}\right. \\ &\quad \left. \times\left(1 \mp \left(1+\frac{1}{3}\left(\frac{r_1}{R_+}\right)^2\right)\left(1-\left(\frac{r_1}{R_+}\right)^2\right)^{1/2}\right)\right] \end{aligned} \quad [A.50]$$

using [A.37] and [A.38] we obtain

$$V = \pi R_o^3 \left[\frac{2}{3} - \cos\theta_c + \frac{1}{3}\cos^3\theta_c + \frac{\delta R}{R_o}\left[\frac{-2 + 2\cos\theta_c + \frac{1}{3}\cos^2\theta_c - \frac{1}{3}\cos^4\theta_c}{\cos\theta_c}\right] + \frac{G}{R_o}\left[\frac{-2 + \cos\theta_c + \frac{4}{3}\cos^2\theta_c - \frac{1}{3}\cos^4\theta_c}{\cos\theta_c}\right] + O(G/R_o)^2 \right] \quad [A.51]$$

using the result

$$\cos\theta_c = \pm\left(1 - \left(\frac{r_1}{R_o}\right)^2\right)^{1/2}, \quad [A.52]$$

where θ_c is the contact angle of the undistorted drop on the substrate.

Since the drop volume must also equal the undistorted volume, viz,

$$V = \pi R_o^3\left(2/3 - \cos\theta_c + \frac{1}{3}\cos^3\theta_c\right), \quad [A.53]$$

we see that

$$\delta R = -G\frac{\left[-2 + \cos\theta_c + \frac{4}{3}\cos^2\theta_c - \frac{1}{3}\cos^4\theta_c\right]}{\left[-2 + 2\cos\theta_c + \frac{1}{3}\cos^2\theta_c - \frac{1}{3}\cos^4\theta_c\right]} = -G\left[1 - \frac{\cos\theta_c}{-2 + 1/3\cos^2\theta_c + 1/3\cos^3\theta_c}\right]. \quad [A.54]$$

Substituting in [A.39] yields

$$z_o = z_o^\infty + H(D_o) + G(D_o)\left[\frac{1}{2}\ln\left(\frac{aD_o}{4R^2}\right) + P(\theta_c)\right], \quad [A.55]$$

where

$$z_o^\infty = R_o(1 - \cos\theta_c) \quad [A.56]$$

is the central height of the undistorted drop and

$$P(\theta_c) = \frac{1}{2}\ln\left(\frac{1 + \mathrm{Cos}\,\theta_c}{1 - \mathrm{Cos}\,\theta_c}\right) + \frac{1 - \mathrm{Cos}\,\theta_c}{[2 - 1/3\cos^2\theta_c - 1/3\cos^3\theta_c]}. \quad [A.57]$$

Substituting this result in [2.1] we obtain

$$X(D_o) = z_o^\infty + D_o + H(D_o) + G(D_o)\left\{\frac{1}{2}\ln\left(\frac{aD_o}{4R_o^2}\right) + P(\theta_c)\right\}. \quad [A.58]$$

REFERENCES

1. Ducker, W. A., Xu, Z., and Israelachvili, J. N. *Langmuir* **10,** 3279 (1994).
2. Fielden, M. L., Hayes, R. A., and Ralston, J., *Langmuir* **12,** 3721 (1996).
3. Butt, H.-J., *J. Colloid Interface Sci.* **166,** 109 (1994).
4. Preuss, M., and Butt, H.-J., *Langmuir* **14,** 3164 (1998).
5. Mulvaney, P., Perera, J. M., Biggs, S., Grieser, F., and Stevens, G. W., *J. Colloid Interface Sci.* **183,** 614 (1996).
6. Snyder, B. A., Aston, D. E., and Berg, J. C., *Langmuir* **13,** 590 (1997).
7. Hartley, P. G., Grieser, F., Mulvaney, P., and Stevens, G. W., *Langmuir* **15,** 7282 (1999).
8. Miklavcic, S. J., Horn, R. G., and Bachmann, D. J., *J. Phys. Chem.* **99,** 16357 (1995).
9. Bachmann, D. J., and Miklavcic, S. J., *Langmuir* **12,** 4197 (1996).
10. White, L. R., *J. Colloid Interface Sci.* **95,** 286 (1983).
11. Solomentsev, Y., and White, L. R., *J. Colloid Interface Sci.* **218,** 122 (1999).
12. Abramowitz, M., and Stegun, I. A., “Handbook of Mathematical Functions.” Dover Pub., New York, 1965.